

REVISITING RAREFIED GAS EXPERIMENTS WITH RECENT SIMULATION TOOLS

ANGELOS G. KLOTHAKIS¹, GEORGIOS N. LYGIDAKIS²,
STAVROS N. LELOUDAS³ AND IOANNIS K. NIKOLOS⁴

¹²³⁴Technical University of Crete
School of Production Engineering and Management
University Campus, Chania, GR-73100, Greece

¹anklothakis@isc.tuc.gr, ²glygidakis@isc.tuc.gr, ³leloudas@isc.tuc.gr, ⁴jnikolo@dpem.tuc.gr

Key words: Rarefied Gas Dynamics, Direct Simulation Monte Carlo, Validation.

Abstract. The Direct Simulation Monte Carlo (DSMC) method was proposed by Graeme Bird in 1970's. It models the gas using simulation particles and samples the flow to obtain its macroscopic properties. At the beginning of 1980's several experiments were conducted in Imperial College, London, in order to provide accurate data for the validation of DSMC codes. These experimental data have not been used for validation purposes for several years, although they have been conducted carefully so as to reduce the experimental error at its minimum. In this work we simulate one of these experiments using SPARTA, a modern DSMC kernel, with advanced molecular collisions model and we compare our results with older simulation results, as well as with the corresponding experimental data.

1 INTRODUCTION

The Direct Simulation Monte Carlo (DSMC) method was first proposed by Graeme Bird in 1970's [1]. When it was introduced it was not widely accepted by the scientific community but as the years passed the method evolved and became a suitable alternative to the use of Navier-Stokes equations mainly in rarefied gas flows. The DSMC method models the fluid using interacting simulation particles, each one of them representing a large number of real fluid particles. These simulation particles are placed inside the computational cells of the simulation domain and are characterized by their position, velocity and internal energy. Then, the simulation particles move with their assigned speeds and collide, while the computational cells are subsequently sampled to obtain the macroscopic properties of the flow.

This method can be applied for several types of rarefied gas flows, usually in high Mach numbers. Due to the complications of the internal energy exchange when a collision occurs, the early molecular models, used in DSMC, were restricted to monoatomic gases. Despite the fact that various collision models have been later developed to deal with polyatomic gases, from empirical to fully quantum-mechanical ones, the problem of selecting one that is most-appropriate for DSMC simulations still remains. The tradeoff between precision and efficiency should be considered wisely, since the algorithm uses many millions of such

simulation particles during a single run.

During the 90's the DSMC method was widely accepted and it was the dominant method for simulating rarefied gas flows [1]. At that period several researchers developed some of the current well known and widely-utilized parallel DSMC solvers. DAC (DSMC Analysis Code) was one of the first parallel codes, which later became the official DSMC code for NASA [2]. SMILE, developed by Ivanov et al. [3], became the official code for the Russian space agencies. MONACO was one of the first DSMC codes which employed a volume grid comprised of unstructured cells [4]; a volume grid with structured cells could also be used [4]. The same period two additional codes were developed, ICARUS [5] and MGDS [6]. ICARUS was developed in Sandia National Laboratories and was used in a wide variety of rarefied gas problems [5]. The MGDS code was developed at the University of Minnesota. The code uses a Cartesian grid but it performs fully automated adaptive mesh refinement during a DSMC simulation. The recent DSMC code SPARTA was developed in the Sandia National Laboratories [7]. This code makes use of the most recent grid adaption techniques, molecular models as well as parallelization techniques, which render the code probably the most computationally-efficient DSMC code currently available [7].

In this work we examine one test case of a hollow cylinder, firstly introduced in 1983 by Davis et al. [8] and experimentally investigated in the Imperial College Hypersonic Nitrogen Wind tunnel. The collision models used at that time to simulate the corresponding test case were the variable- ϕ Morse potential [8], the hybrid Morse potential [8] and the inverse-power variable- ϕ [8].

2 COLLISION MODELING

The collision models in the DSMC method are separated in two categories. Impulsive models, employing approximations to classical or quantum-mechanical representations of the collision, and phenomenological models, where local relaxation concepts are used to calculate the energy exchanges [9]. The first model introduced to the DSMC method was the hard sphere model [9, 10, 11]. This model treats molecules as hard spheres which collide (as shown in Figure 1) when their distance decreases to

$$r = \frac{1}{2}(d_1 + d_2) = d_{12} \quad (1)$$

where d_1 and d_2 are the diameters of the colliding molecules. Its main advantage is that it uses a finite cross-section defined by

$$\sigma_T = \pi d_{12}^2 \quad (2)$$

and an easy calculation of the collision. The scattering of hard sphere molecules is isotropic in the center-of-mass frame of reference. In other words, all directions are equally likely for c_r^* , where c_r^* is the magnitude of particle's velocity. In the hard sphere model, the viscosity and diffusion cross-sections are defined respectively as

$$\sigma_\mu = \frac{2}{3} \sigma_T \quad (3)$$

and

$$\sigma_M = \sigma_T \quad (4)$$

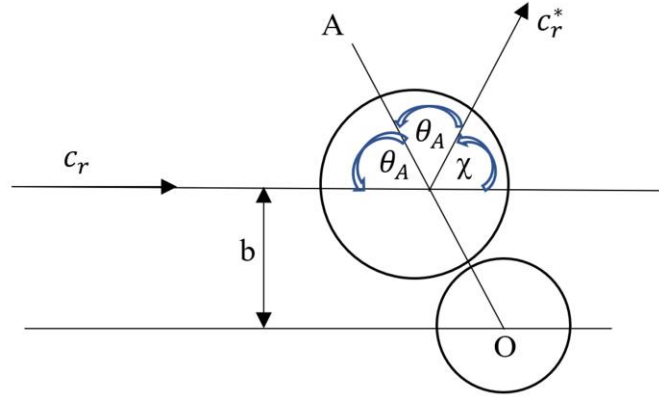


Figure 1: Collision geometry of the hard sphere model

3.1 The Variable Hard Sphere model (VHS)

The main characteristics of the hard sphere model are the finite cross-section and the isotropic scattering in the center-of-mass frame of reference. Unfortunately, this scattering law is unrealistic. However, the main drawback of the hard sphere model is the resulting dynamic viscosity. According to Bird [1], a molecular model for rarefied gas flows should reproduce the dynamic viscosity of the real gas and its temperature dependence. The viscosity of the hard sphere model results to be proportional to the temperature to the power of 0.5, whereas real gases have powers of the order of 0.75. The main reason for this absence of accuracy is that the cross-section of the particles is independent of the relative translational energy

$$E_t = \frac{1}{2} m_r c_r^2. \quad (5)$$

The real cross-section depends on this relative velocity c_r . Because of the inertia, the change in the trajectories decreases when the relative velocity increases, so the cross-section must decrease when c_r increases. A variable cross-section is thus required to match the power of 0.75 that is a characteristic of real gases. This led to the variable hard sphere model (VHS) [9, 10, 11]. In this model, the molecule is modeled as a hard sphere with a diameter d that is a function of c_r , using an inverse power law

$$d = d_{ref} \left(\frac{c_{r,ref}}{c_r} \right)^\xi \quad (6)$$

where the subscript *ref* devotes reference values; d_{ref} corresponds to the effective diameter at relative speed $c_{r,ref}$ and ξ is the VHS parameter depending on the particle species. For a particular gas the reference values are defined by the effective diameter at a particular temperature. In the VHS model the deflection angle is given by

$$x = 2 \cos^{-1} \frac{b}{a} \quad (7)$$

The VHS model leads to a temperature dependence of the coefficient of viscosity such that

$$\mu \propto T^\omega \quad (8)$$

where T is the temperature and,

$$\omega = \frac{1}{2} + \xi \quad (9)$$

3.2 The Variable Soft Sphere model (VSS)

The most recent popular model used in DSMC simulations is the Variable Soft Sphere model (VSS) [4]. In this model the deflection angle compared to the VHS is modified as

$$x = 2 \cos^{-1} \left(\left(\frac{b}{a} \right)^{1/a} \right) \quad (10)$$

where a is the VSS scattering parameter. The total collision cross-section of a variable soft sphere is given by $\sigma_T = \pi d^2$. As a result this leads to the following dynamic viscosity expression for a VSS gas,

$$\mu = \frac{5}{16} \frac{(\alpha + 1)(\alpha + 2) \sqrt{\pi m k} \left(\frac{4k}{m} \right)^\xi T^{\frac{1}{2} + \xi}}{\alpha \Gamma(4 - \xi) \sigma_{T,ref} c_{r,ref}^{2\xi}} \quad (11)$$

Similarly to the VHS model, the viscosity is proportional to $T^{\frac{1}{2} + \xi}$ and the parameter ξ is chosen as in the VHS model. The diffusion coefficient in a VSS gas mixture is given [12]

$$D_{12} = \frac{3}{16} \frac{(a_{12} + 1) \sqrt{\pi} \left(\frac{2kT}{m_r} \right)^{\frac{1}{2} + \xi_{12}}}{\Gamma(3 - \xi_{12}) n \sigma_{T,ref,12} c_{r,ref}^{2\xi_{12}}} \quad (12)$$

For a simple gas with viscosity μ_{ref} and self-diffusion coefficient $D_{11,ref}$ at the reference temperature T_{ref} the effective diameters d and d_{ref} based on the viscosity and diffusion are given [12]

$$d = \sqrt{\frac{5}{16} \frac{(a + 1)(a + 2) \sqrt{m/\pi} (kT_{ref})^{\xi + 1/2}}{\alpha \Gamma(4 - \xi) \mu_{ref} E_t^\xi}} \quad (13)$$

$$d_{11} = \sqrt{\frac{3}{8} \frac{(a + 1) (kT_{ref})^{\xi + 1/2}}{\Gamma(3 - \xi) \sqrt{\pi m} D_{11,ref} E_t^\xi}} \quad (14)$$

respectively. By requiring equity for the two diameters, α may be determined as

$$\alpha = \frac{10\rho D_{11,ref}}{6(3 - \xi)\mu_{ref} - 5\rho D_{11,ref}} \quad (16)$$

Consequently, the VSS model reflects the diffusion process more precisely than the VHS one and is thus more favorable for the analysis of diffusion phenomena. A limitation of the model is that constant values for α are generally only valid in a certain temperature range. It has to be noted that the VHS and VSS models both approximate the realistic inverse power law model. Details of the older models used in this work, namely the variable- φ Morse

potential, the hybrid Morse potential, and the inverse-power variable- φ , can be found in [13, 14]. In brief these older models treat the individual collisions as inelastic with probability φ or completely elastic with probability $1 - \varphi$. The constant φ is called the exchange restriction factor and ranges between 0.1 and 1. During an inelastic collision, the total energy is redistributed between the translational and rotational modes, according to probabilities derived from the equilibrium distribution [12].

4 THE HOLLOW CYLINDER EXPERIMENT

In 1983, to access the accuracy of the variable- φ and hybrid models in practical applications, comparisons have been carried-out between computational and experimental results; two body shapes were used, namely a hollow cylinder and a blunt cone; These particular body shapes have been chosen in order to minimize experimental error [8]. The method used in order to obtain the experimental results was the electron-beam fluorescence technique. This method avoids interference caused by physical probes, which, in rarefied gases, can be excessive [8]. In this work, only the hollow cylinder case will be considered.

In the flow developed on the hollow cylinder we expect viscous effects to dominate. However, this type of shapes are dogged by undesirable three-dimensional flow effects, which in the rarefied regime can be troublesome [15]. The experiment was conducted in the Imperial College Nitrogen Wind Tunnel, which operates between Mach number 20 and 24 [8]. Mean free paths λ_∞ of 0.5 mm can be achieved within the wind tunnel [8]. The model was water cooled and constructed using tellurium-copper alloy [8]. The hollow cylinder has 44 mm diameter at the leading edge, while it is 150 mm long. The leading edge is sharp and chamfered at 10° at the inner surface, while the outer surface was given a slight taper of 1° [8]. This was necessary because the conicity of the undisturbed tunnel flow had a 1° outflow at the model's leading edge [8]. The model's geometry is presented in Figure 2.

As far as the electron-beam is concerned, the method used was the one described in [16]. A beam of electrons was fired into the gas from a 30 kV source outside the tunnel. This caused a fluorescent glow, the intensity of which at points along the beam gave a measure of gas density [17]. On the surface of the hollow cylinder a thin layer of graphite was embedded, making possible to fire the beam directly at the model without the effect of an increased glow near the surface from the reflected particles. As mentioned in [8], a high-thermal conductivity adhesive was used to hold the graphite in place and a temperature rise of less than 0.3 K was estimated due to aerodynamic heating.

The upstream boundary conditions were set in this work so as to match those measured in [8]. The boundary conditions and the DSMC code parameters can be found in Tables 1 and 2 respectively. The DSMC code used in this work is SPARTA, developed in Sandia National Laboratories [7]. It is a high-efficiency parallel open-source DSMC code distributed under the terms of the GPL license. To run a simulation with SPARTA the corresponding parameters have to be defined first, i.e., the simulation box (computational domain), the grid, the internal boundaries (inside the simulation box), the particle species (e.g., oxygen, nitrogen, ions) and the initial population of the particles. For a two-dimensional run, the simulation box is defined by the coordinates of the boundaries; minimum and maximum coordinates in x- and y- axis. For a three-dimensional simulation the coordinates of two more boundaries have to be defined (including coordinates in z-axis). As far as the computational discretization is concerned,

SPARTA employs a hierarchical Cartesian grid strategy. The simulation domain is considered initially as a single grid cell (level 0). The cell is divided in N_x by N_y by N_z cells at level 1, while at next each one of these cells can be further divided into smaller ones at different levels. The properties of the particle species, such as their diameter and molecular weight, are acquired from an additional appropriately formatted file. Finally, the initial population of the particles is defined from the F_{num} number, denoting the number of real particles represented by a single simulation particle. As far as initialization of the procedure is concerned, the corresponding velocities are retrieved from a Maxwellian speed distribution function [7].

The domain used in this simulation spans from -0.02 m to 0.15 m along the x-axis and from 0 m to 0.1 m along the r-axis. To divide the computational domain, a Cartesian grid was used, with 350 and 180 cells along the x- and r-axis respectively. Around the hollow cylinder geometry the grid cells were further refined to 10 by 10 cells. A detail of the aforementioned grid can be seen in Figure 2. In order for the results to be comparative to the older ones, since in [2] the number of particles used is not mentioned, in this work the number of particles were kept to the minimum number required for a successful DSMC simulation. It has to be noted that better results can be produced if the number of particles is increased. The simulation was performed on a DELLTM R815 PoweredgeTM Server with four AMD OpteronTM 6380 16-core processors. The initial grid was decomposed and distributed to 60 cores and the simulation required approximately 5 days to complete.

To speed-up the simulation, the recursive coordinate bisectioning method (RCB) was used, in which the processors are assigned compact clumps of grid cells [7]. To every cell a weight coefficient is assigned, hence, dynamic load balancing aims to assign equal total weights to all processors. This weight coefficient can be defined in various ways, e.g., if it is set equal to unity, each processor is assigned the same number of cells, while if it is set equal to the number of the included particles, the same number of particles is assigned to all the processors.

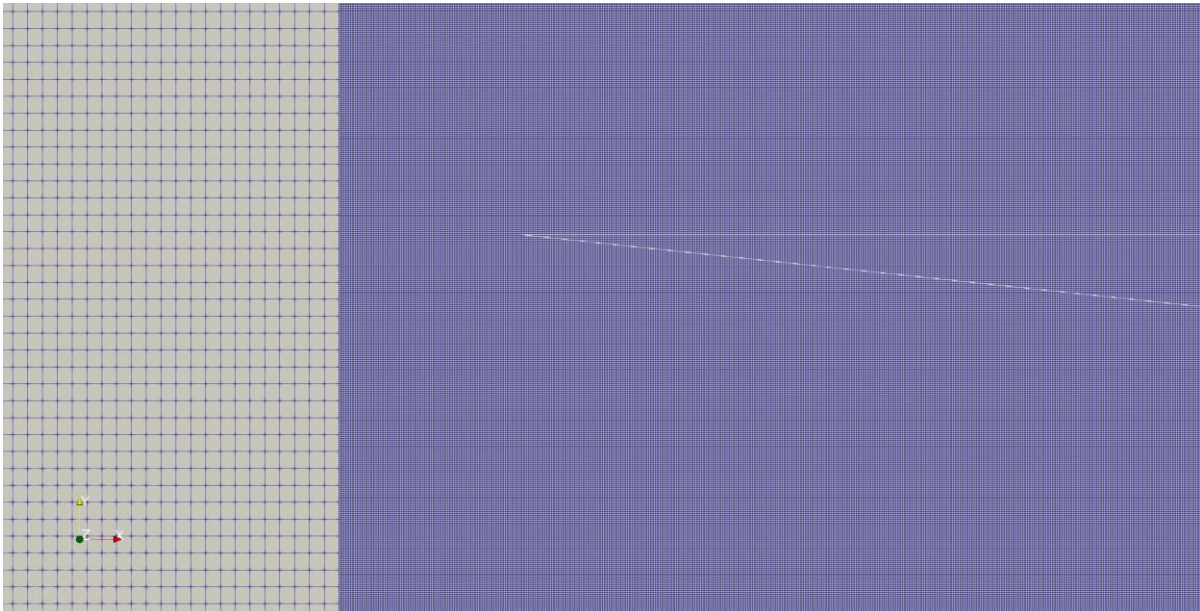


Figure 2: DSMC grid detail

Table 1: Flow conditions

V_∞ (m/s)	2780
ρ_∞ (<i>particles</i> /m ³)	3.192x10 ²¹
T_∞ (K)	95.6
T_w (K)	290
Mean free path (λ_∞) (mm)	0.33

Table 2: DSMC code parameters

V_∞ (m/s)	2780
F_{num}	1057.48
Timestep (s)	3x10 ⁻⁸
Transient period (steps)	200,000
Sampling period (steps)	50,000

5 NUMERICAL RESULTS

The SPARTA code simulated the flow in an axisymmetric domain by utilizing the VSS model. In this simulation the main objective was to calculate the flow density in different positions on the upper surface of the hollow cylinder. The measuring positions were defined according to [8] and can be seen in Figure 3. At this point it must be noted that the measuring took place along the whole length of the lines shown, from the surface of the cylinder up to the outside shock area. Furthermore, the simulation data, produced by the older models have been taken from [8]. In this work only the results for the VSS model were produced using the SPARTA kernel, and thus compared to the older models. The density contours computed by SPARTA are presented in Figure 4: the flow develops from a kinetic region around the cylinder's leading edge to a fully shock and viscous layer downstream. The shock developed around the cylinder is produced by the displacement effect of the viscous layer. Thus, within it the density rises quickly and steeply to a peak value. This is because of the interference of the shock's structure with the non-equilibrium viscous layer that exists in the space between the shock and the cylinder's surface [8].

Furthermore, the measuring positions were defined as the ratio of the x distance divided by the mean free path (x/λ_∞). The y -axis (r -axis) of the plots was defined in the same manner such as y/λ_∞ . The four measurement positions are summarized in Table 3. We can clearly observe that the model that gives better overall agreement is the newer VSS one, followed by the hybrid Morse, the variable- ϕ Morse and, finally, the inverse power variable- ϕ model. The results for the VSS model show that the flow develops fast with steep gradients and a strong

shock being close to the measured one. In contrast, the inverse variable- ϕ model accounts for a weaker shock and a slower developing flow. This was expected, because the VSS and the Morse potential models give a better prediction of viscosity over a wider range of temperatures.

At position 1, which is close to the leading edge and is within the kinetic region of the flow, both VSS and variable- ϕ models are in very good agreement with the experimental results. As the flow develops further, on the cylinder's external surface the differences between the models can be more clearly observed. Since the merged layer is essentially a matching between the strongly interacting viscous boundary layer generated by the particles reflected from the body and the developed shock, the conditions downstream of the shock are a very sensitive indicator [8]. In the second measurement position we can see that the VSS model provides a better agreement with the experimental data than the hybrid Morse potential one, especially at the peak density point.

Finally, as we move forward to the third and fourth positions, shown in Figure 6a and 6b respectively, it can be observed that in the third position VSS and Hybrid Morse models produced close results. In addition, in the fourth position the VSS model slightly over-predicts the peak density point and the density after the peak point, whereas has a good agreement at the points before that. Since the number of particles used during the simulation is not mentioned in [8], in this work the simulation particles were kept around the minimum number of particles required for the model to run a successful simulation. As far as the third position is concerned, the VSS model produces a slightly better result at the density peak point, under-predicts at the area outside the shock region and has a very good agreement with the Hybrid Morse model before the density peak point.

Table 3: Measurement positions [8]

Position Number	x/λ_∞
1	14.9
2	44.6
3	89.6
4	140.0

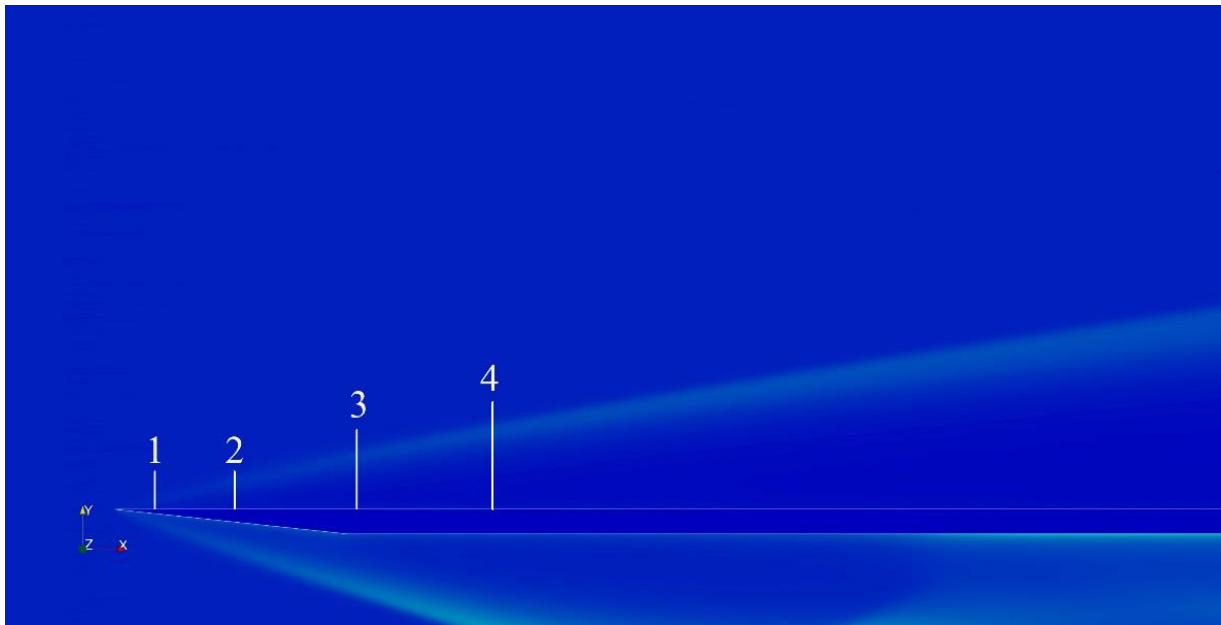


Figure 3: Measurement positions

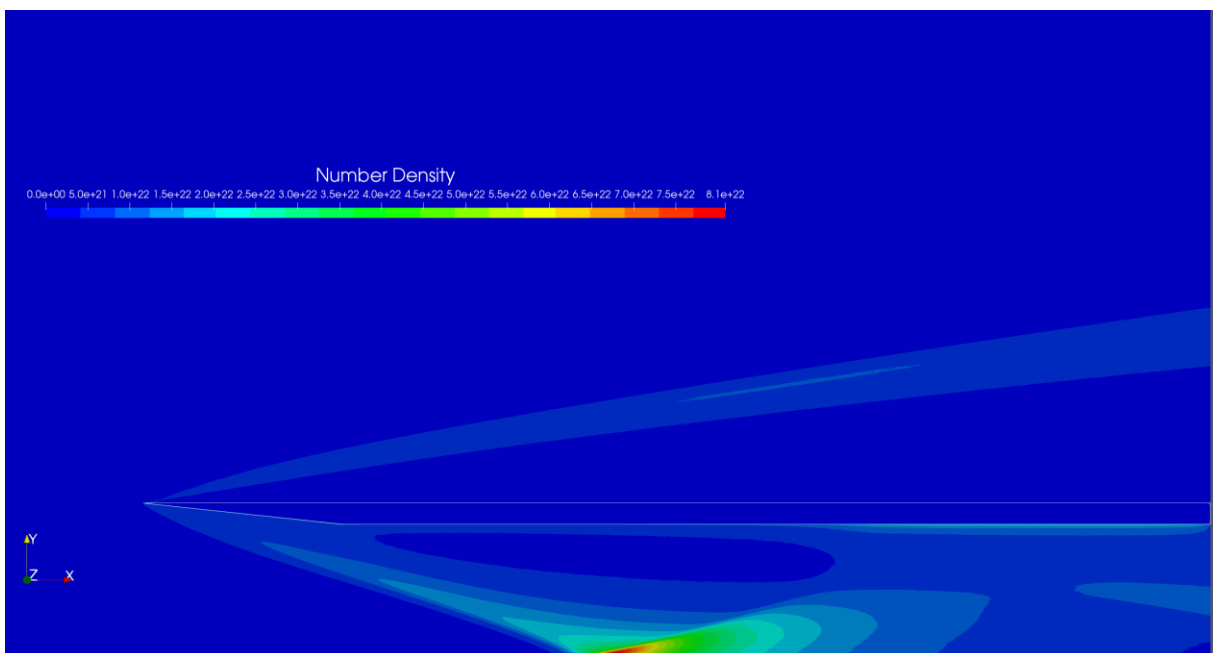


Figure 4: Density contours

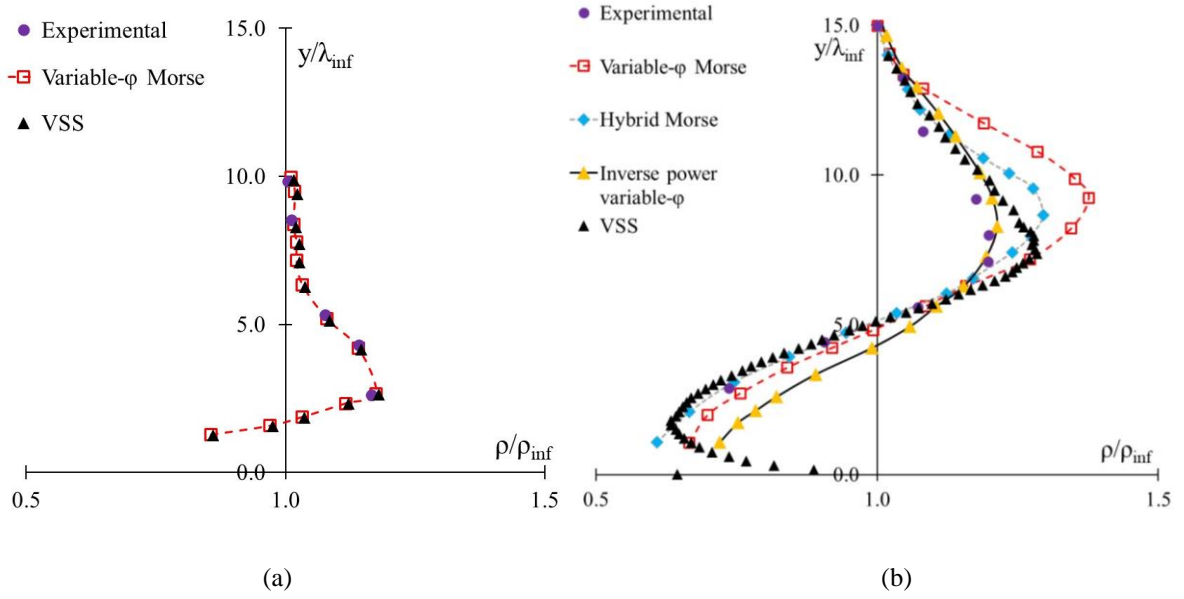


Figure 5: (a) Density plot for position 1; (b) Density plot for position 2 (points for variable- ϕ Morse, Hybrid Morse, and Inverse power variable- ϕ models were extracted from [8])

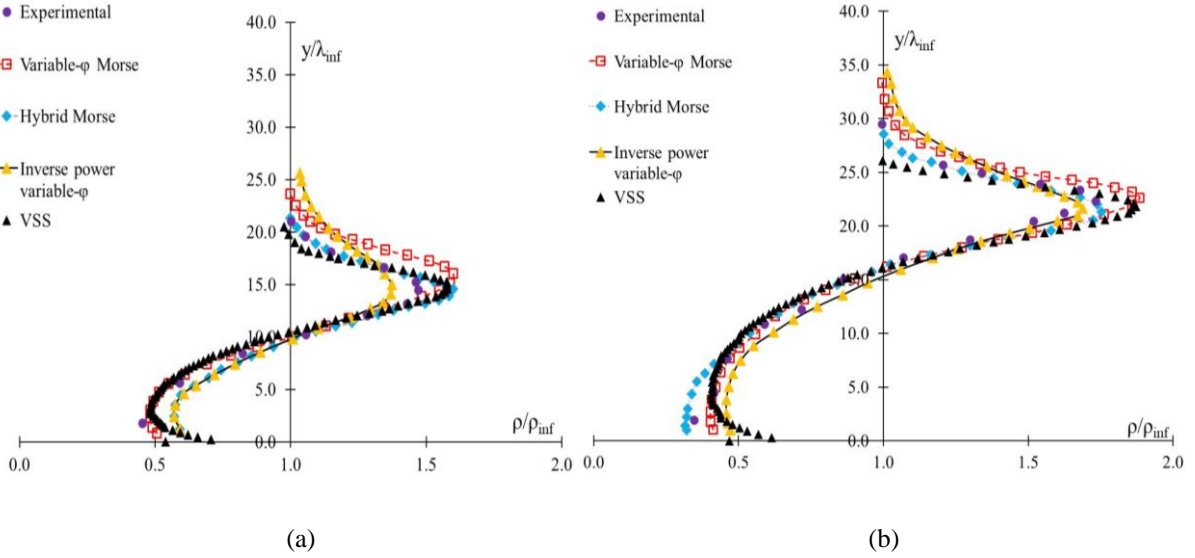


Figure 6: (a) Density plot for position 3; (b) Density plot for position 4 (points for variable- ϕ Morse, Hybrid Morse, and Inverse power variable- ϕ models were extracted from [8])

6 CONCLUSIONS

In this work the DSMC code SPARTA was used to simulate a hypersonic rarefied gas flow test case. Three old DSMC collision models (variable- ϕ Morse potential, Hybrid Morse potential, and inverse-power variable- ϕ) were compared with a more recent one (VSS) against experimental results. Generally, a good agreement was observed between the Hybrid Morse potential and the VSS models, although the VSS one is expected to produce better results with

a higher number of particles than those used in this work. The hollow cylinder geometry is an axisymmetric equivalent of the flat plate geometry. The fastest model, as mentioned in [8], is the inverse-power variable- φ one, which provided tolerable results in comparison with the experimental data.

As there is no evidence of the simulation time required we cannot say how long the original simulations required to reach a solution; the SPARTA code with the VSS model required 5 days in 60 cores; the VSS model is able to produce good results, although it is not a computationally cheap model. Further tests will be performed using more particles, as well as for lower densities, in order to demonstrate how the computational time varies with gas density. On-going work includes the comparison of the VHS model simulation results with the available experimental data, while other cases from the same batch of experiments are also under investigation.

REFERENCES

- [1] Bird, G.A. *Molecular gas dynamics and the direct simulation of gas flows*. Clarendon Press, Oxford (1994).
- [2] LeBeau, G.J. A parallel implementation of the direct simulation Monte Carlo method. *Computer Methods in Applied Mechanics and Engineering* (1999) **174**:319-337.
- [3] Ivanov, M., Markelov, G. and Gimelshein, S. Statistical simulation of reactive rarefied flows: Numerical approach and applications. *Proceedings of the 7th AIAA/ASME Joint Thermophysics and Heat Transfer Conference*, Albuquerque, NM, U.S.A. (1998).
- [4] Dietrich, S. and Boyd, I.D. Scalar and parallel optimized implementation of the direct simulation Monte Carlo method. *Journal of Computational Physics* (1996) **126**:328-342.
- [5] Bartel, T.J., Plimpton, S. and Gallis, M.A. Icarus: A 2-D Direct Simulation Monte Carlo (DSMC) code for multi-processor computers, User's Manual – v 10.0. Sandia National Laboratories, Sandia Report SAND2001-2901 (2001).
- [6] Gao, D. and Schwartzentruber, T.E. Optimizations and OpenMP implementation for the direct simulation Monte Carlo method. *Computers & Fluids* (2011) **42**:73-81.
- [7] Gallis, M.A., Torczynski, J.R., Plimpton, S.J., Rader, D.J. and Koehler, T. Direct Simulation Monte Carlo: The quest for speed. *AIP Conference Proceedings* (2014) **1628**:27.
- [8] Davis, J., Dominy, R.G, Harvey, J.K. and Macrossan, M.N. An evaluation of some collision models used for Monte Carlo calculations of diatomic rarefied hypersonic flows. *Journal of Fluid Mechanics* (1983) **135**:355-371.
- [9] Bird, G.A. Breakdown of translational and rotational equilibrium in gaseous expansions. *AIAA Journal* (1970) **8**:1998-2003.
- [10] Borgnakke, C. and Larsen, P.S. Statistical collision model for Monte-Carlo simulation of polyatomic gas mixture. *Journal of Computational Physics* (1975) **18**:405-420.
- [11] Larsen, P.S. and Borgnakke, C. Statistical collision model for simulating polyatomic gas with restricted energy exchange. *Proceedings of the 9th Symposium in Rarefied Gas Dynamics*, Vol. I, paper A7, Germany (1974).
- [12] Koura, K. and Matsumoto, H., Variable soft sphere molecular model for air species. *Physics of Fluids A: Fluid Dynamics* (1992) **4**:1083-1085.

- [13] Pullin, D.I. Kinetic models for polyatomic molecules with phenomenological exchange. *Physics of Fluids* (1978) **21**:209-216.
- [14] Pullin, D.I. and Harvey, J.K. A numerical simulation of the rarefied hypersonic flat plate problem. *Journal of Fluid Mechanics* (1976) **78**:689-707.
- [15] Moss, J.N and Bird, G.A. Direct Simulation Monte Carlo simulations of hypersonic flows with shock interactions. *AIAA Journal* (2005) 43:2565-2573.
- [16] Harvey, J.K., Jeffery, R.W. and Uppington, D.C. The Imperial College graphite heated hypersonic wind tunnel. Ministry of Defense, Aeronautical Research Council Reports and Memoranda, R. & M. 3701 (1971).
- [17] Muntz, E.P. Measurement of rotational temperature, vibrational temperature, and molecular concentration, in non-radiating flows of low density nitrogen. Institute of Aerophysics, University of Toronto, UTIA Report No. 71, AFSOR TN 60-499 (1961).